Nanoscale Advances

ROYAL SOCIETY OF CHEMISTRY

PAPER

View Article Online
View Journal | View Issue

Cite this: *Nanoscale Adv.*, 2020, **2**, 4770

One-pot sustainable preparation of sunlight active ZnS@graphene nano-composites using a Zn containing surface active ionic liquid†

Komal Arora,[a] Gurbir Singh,[b] Sekar Karthikeyan [c] and Tejwant Singh Kang *[a]

Received 14th June 2020
Accepted 10th August 2020

DOI: 10.1039/d0na00486c

rsc.li/nanoscale-advances

Herein we report a facile and sustainable method for the preparation of ZnS@graphene nano-composites (NCs). An appreciable amount of graphene is obtained by liquid-phase exfoliation using a zinc-containing surface active ionic liquid (SAIL). It is followed by *in situ* preparation of ZnS quantum dot (QD) decorated graphene sheets at room temperature for the first time. The employed method is distinct from all previous reports, as we have employed graphene instead of graphene oxide (GO) or reduced graphene oxide (rGO) and used relatively fewer chemicals. Further, a SAIL is employed as a precursor of Zn^{2+} as well as a template for the preparation of ZnS QDs onto graphene. The prepared ZnS@graphene NCs show enhanced photocatalytic performance for the degradation of Rhodamine B dye under sunlight and ciprofloxacin antibiotic under visible light as compared to bare ZnS QDs. The better photocatalytic activity of the NCs under visible light compared to that reported in the literature along with the ease of preparation is advantageous for scaling-up the process.

1. Introduction

Water pollution, due to the release of organic pollutants such as dyes, organic chemicals, and antibiotics, *etc.* from industries, has a deleterious impact on the aquatic organisms and mankind.[1,2] One of the promising solutions to solve the water crisis and environmental problems is the utilization of photocatalysts.[3] Photocatalysts absorb light energy which results in generation of reactive species, which degrades the organic pollutants present in wastewater.[3] Semiconductor photocatalysts (TiO_2, ZnS, ZnO, CdS, SnO_2, and ZnSe, *etc.*) have been extensively studied to achieve these goals.[4] Among these photocatalysts, ZnS QDs are non-toxic, cost-effective in preparation, and can be prepared in large quantities.[5,6] However, a large band-gap (~3.7 eV) of ZnS QDs renders them applicable only when excited in the UV range.[7] This would be a limitation for photocatalytic applications of ZnS QDs in large water bodies using sunlight as UV radiation corresponds to ~5% of the solar spectrum.

Recently, the coupling of graphene with ZnS QDs has been found to be a promising concept for enhancing the photocatalytic activity of ZnS QDs.[8–10] Graphene provides not only a larger surface area for the adsorption of pollutants but also increases the electron density in the conduction band of the photocatalyst by interfacial charge transfer.[10–14] This enhances the photocatalytic efficiency and makes the photocatalysis process feasible under visible light *via* decreasing the band gap of ZnS adsorbed onto graphene.[9–11] The graphene–ZnS nanocomposites (NCs) reported in the literature,[10–13] involve the use of either graphene oxide (GO) or reduced graphene oxide (rGO) prepared by Hummer's method.[15] Although this method is beneficial, however, it is multistep and employs many toxic reagents. Nonetheless, the oxidation process leaves a considerable number of structural defects in graphene that disturb its electronic properties. This could partially hinder the interfacial charge transfer between rGO and the adsorbed photocatalyst, which would result in the suppression of photocatalytic efficiency. Therefore, there is a need to devise new methods for preparing graphene-semiconductor NCs using graphene instead of GO and rGO, with a reduced number of preparatory steps and chemicals employed. This would not only add to sustainability but the graphene-based semiconductor NCs are also expected to show better photocatalytic properties due to fewer structural defects and better electronic properties of graphene as compared to GO or rGO.

Herein, we adopted a new sustainable approach for liquid-phase exfoliation of defect-free non-oxidized graphene followed by *in situ* preparation of ZnS quantum dot (QD) decorated graphene sheets employing an imidazolium-based zinc-containing surface active ionic liquid (SAIL), $[C_{16}mim][ZnCl_3]$ (Scheme 1).

[a]*Department of Chemistry, University Grants Commission (UGC) Centre for Advanced Studies-II, Guru Nanak Dev University, Amritsar-143005, Punjab, India. E-mail: tejwant.chem@gndu.ac.in*

[b]*Department of Earth Resources Engineering, Faculty of Engineering, Kyushu University, 744 Motooka, Nishi-ku, Fukuoka 819-0395, Japan*

[c]*Department of Chemistry and Biochemistry, Graduate School of Engineering, Kyushu University, 744 Motooka, Nishi-ku, Fukuoka 819-0395, Japan*

† Electronic supplementary information (ESI) available: Annexure S1; Fig. S1–S10. See DOI: 10.1039/d0na00486c

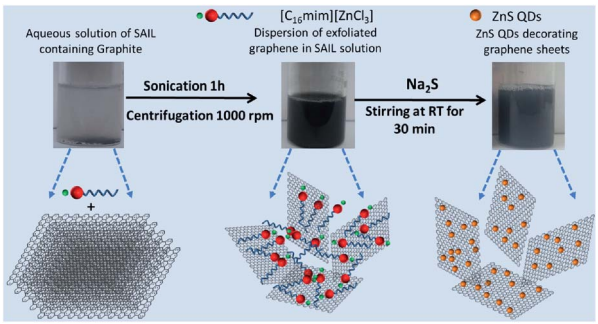

Scheme 1 Photographs and schematic representation of exfoliation of graphene and subsequent preparation of ZnS QD decorated graphene.

SAILs are a class of ionic liquids (ILs)[16] which exhibit surfactant like behaviour[17] and many a times show even better surface-active properties as compared to conventional ionic surfactants. The metal-containing SAIL for the exfoliation of graphene not only exfoliates graphene in considerable quantity and quality in the form of a stable dispersion but also acts as a precursor of Zn^{2+} as well as the template for subsequent preparation of ZnS QDs onto graphene at room temperature. This reduces the use of toxic chemicals, reduces the number of steps, and allows *in situ* preparation of ZnS QDs. In the past, conventional surfactants,[18] polymer–ILs,[19] and ILs having aromatic anions[20] have been employed to exfoliate graphene. However, metal (M) containing SAILs to prepare metal-based nano-materials appended to graphene have never been explored. Thus, the prepared graphene@ZnS NCs are tested for the photocatalytic degradation of Rhodamine B under sunlight and an antibiotic, ciprofloxacin (CIP), under visible light, which further widens the applicability arena of the prepared NCs.

2. Experimental

2.1. Materials

Graphite (+100 mesh, product no. 332461), sodium sulphide nonahydrate ($Na_2S{\cdot}9H_2O$) (>99%), 1-methylimidazole (>99%), 1-chlorohexadecane (>95%) and Rhodamine B (>95%) were purchased from Sigma Aldrich and used as received. Zinc chloride ($ZnCl_2$) (>99%) was purchased from Loba Chemie. Dichloromethane (AR grade), diethyl ether (AR grade), hexane (AR grade), and ethyl acetate (AR grade) were purchased from SD Fine-Chem. Ltd., India.

2.2. Exfoliation and characterization of graphene sheets

The used SAIL, $[C_{16}mim][ZnCl_3]$, was synthesized and characterized using the method reported in the literature.[15] 2.5 mg mL^{-1} of pristine graphite was sonicated for 1 hour in an aqueous solution of SAIL, $[C_{16}mim][ZnCl_3]$, at three different concentrations (1, 5 and 10 mmol L^{-1}). A low energy bath sonicator (Citizon CUB2.5, Power 50 W, Frequency 40 kHz) was used for this purpose. After sonication, the formed suspension of graphene was centrifuged at 1000 rpm for 1 hour to remove unexfoliated graphite settled at the bottom of the vial. 80% of the dark supernatant containing graphene sheets was pipetted out carefully and used for further studies. UV-visible absorption spectra of the thus obtained supernatant were measured using a UV-Vis spectrophotometer (Cary 5000 UV-Vis-NIR) in the wavelength range of 350–800 nm using a quartz cuvette having path length of 1 cm. X-ray diffraction patterns of the graphite used and exfoliated graphene sheets were recorded on a Rigaku Xpert Pro X-ray diffractometer having a Cu-target ($\lambda \sim 0.154$ nm) in the 2θ range of 5–80° with a step size of 0.02°. Raman spectra of graphite and exfoliated graphene sheets after washing with double distilled water and methanol followed by air drying for 24 h were recorded on a Renishaw Raman spectrophotometer in the range of 3500–300 cm^{-1} using an Ar-ion laser at a wavelength of 514 nm. X-ray photoelectron spectroscopy (XPS) spectra were recorded on a Kratos Axis His spectrometer with a monochromated Al Kα X-ray source operated at 90 W with magnetic focusing and a charge neutralizer. Spectra were fitted using CasaXPS of version 2.3.16, with energy referencing to adventitious carbon at 284.6 eV. Zeta (ζ)-potential measurements were performed using a light scattering apparatus (Zetasizer, nanoseries, nano-ZS, Malvern Instruments), equipped with a built-in temperature controller, having an accuracy of $\pm$0.1 K, at a scattering angle of 173° using a dip cell (ZEN-212). ^{1}H NMR and 2D ^{1}H–^{1}H NOESY experiments were performed on a Brüker Ascend 500 Spectrometer (AVANCE III HD console) with water suppression in a 10% D_2O–90% H_2O mixture. Phase-sensitive 2D ^{1}H–^{1}H NOESY spectra with solvent suppression were recorded with 32 scans and a mixing time of 500 ms. The morphology and lattice structure of exfoliated graphene sheets were investigated by using a JEM-2100 transmission electron microscope (TEM) at a working voltage of 200 kV. For the TEM measurements, the obtained NCs were dispersed in ethanol by ultrasonication in a bath sonicator for 10 minutes. A drop of dispersion was placed on the carbon-coated grid (300 mesh), and the samples were dried at room temperature for 24 hours before the measurements. Atomic force microscopy (AFM) was conducted in tapping mode on an Anton Parr Tosca Series 400. Samples were dropped cast on the mica surface and dried at room temperature for 24 hours before the measurements.

2.3. Preparation of ZnS@graphene nanocomposites (NCs)

The concentration of $[C_{16}mim][ZnCl_3]$ in aqueous solutions containing exfoliated graphene sheets was increased from 5 mmol L^{-1} to 50 mmol L^{-1} for the preparation of ZnS quantum dots (QDs). To this dispersion, an equimolar amount of Na_2S was added, and the resultant dispersion was stirred at 25 °C for 30 min. This resulted in the formation of ZnS quantum dot (QD) decorated graphene sheets (ZnS@G). Thus, the prepared ZnS@G NCs were washed several times with distilled water and methanol to remove the formed by-products and residual $[C_{16}mim][ZnCl_3]$. ZnS QDs were also prepared by following the same procedure in the absence of graphene sheets (ZnS) for comparison.

2.4. Characterization of the prepared ZnS@G NCs

The structural characterization of the thus prepared NCs was performed using XRD, Raman spectroscopy, TEM, and UV-

Visible spectroscopy, similar to the characterization of exfoliated graphene sheets. Photoluminescence spectra of the prepared NCs and bare ZnS were recorded on a Horiba Fluorolog spectrophotometer at an excitation wavelength of 320 nm employing an excitation and emission slit width of 1 nm each.

The measurements were made using a quartz cuvette of path length 1 cm in the wavelength range of 350–500 nm. For both UV-Vis and photoluminescence measurements, spectra were recorded by dispersing an equal amount of the ZnS@G NCs and ZnS QDs in ethanol as solvent.

2.5. Photocatalytic degradation of the Rhodamine B (RhB) dye

20 mg of the prepared catalyst was added to 30 mL of 1×10^{-5} M RhB solution in water. Before sunlight irradiation, the solution was magnetically stirred in the dark for 30 min to reach adsorption–desorption equilibrium. The solutions were then irradiated under sunlight, having a normal irradiance value of ~5.90 kW h per m^2 per day. The absorbance was recorded, at a certain time interval, in a scanning range of 400–700 nm with a scan speed of 600 nm min^{-1}. Reaction rates for photodegradation of RhB were determined by employing the first-order rate equation:

$$\ln C_0/C_t = kt \quad (1)$$

where C_0 and C_t are the concentrations at time = 0 and t, respectively. k is the first-order rate constant (min^{-1}). From the slope of the linear plot between $\ln C_0/C_t$ *vs.* t, the rate constant (k) was calculated.

2.6. Ciprofloxacin (CIP) photodegradation experiment

15 mg of photocatalysts were dispersed in 50 mL of 0.0181 mM CIP solution in a 250 mL photo-reactor and sonicated for 10 min to ensure complete dispersion. Prior to light illumination, the mixture was stirred in the dark for 1 hour to reach adsorption–desorption equilibrium. After this process, 1 mL of the sample was taken for HPLC analysis (Annexure S1, ESI†), and then the sample was continuously stirred under visible light irradiation (cut-off filter $\lambda > 420$ nm; temperature maintained at 25 °C, stirring speed 500 rpm; light intensity 1.82 mV cm^{-2}). Samples were collected at certain time intervals using a CPO20AN filter for all samples including the initial sample. Transient photocurrent and electrochemical impedance spectroscopy (EIS) measurements were conducted by using an electrochemical instrument in 0.5 M aqueous Na_2SO_4 solution in a single compartment quartz cell. A three-electrode cell system was applied with 10 mg of samples on a Pt wire as the counter electrode, FTO glass as the working electrode, and Ag/AgCl as the reference electrode.

3. Results and discussion

The amount of graphene exfoliated was determined using gravimetric analysis.[21] At a $[C_{16}mim][ZnCl_3]$ concentration of 5 mmol L^{-1}, maximum exfoliation of graphene (0.6 mg mL^{-1}) is observed (Fig. S1, ESI†). The amount of exfoliated graphene is comparable or better than that in some literature reports.[18] As the maximum exfoliation is observed at 5 mmol L^{-1} of $[C_{16}mim][ZnCl_3]$, therefore, the graphene exfoliated only at this concentration is characterized and discussed in detail. The absorption coefficient, α, has been calculated from the slope obtained by linear fitting between the absorbance at 660 nm divided by the path length, (A/l), *vs.* concentration of exfoliated dispersed graphene sheets (C_G) (Fig. 1A). The obtained α is 542 L g^{-1} m^{-1}, which indicates that the larger number of graphene sheets that are smaller in size and thickness are present.[22] Absorbance spectra of exfoliated graphene sheets at different graphene concentrations (inset of Fig. 1A) show a flat and featureless band, which is characteristic of graphene and other 2D transition metal dichalcogenides.[21]

The crystalline nature of exfoliated graphene sheets has been studied by XRD (Fig. 1B). Pristine graphite shows a sharp and robust peak at $2\theta \sim 26.5°$ and 54.6° corresponding to (002) and (004) diffraction planes, respectively.

A sharp decrease in intensity of the diffraction peak at ~26° with the disappearance of a band at $2\theta \sim 54°$ is observed in the case of exfoliated graphene. This supports the fact that graphite has been successfully exfoliated into few-layer graphene sheets.[24] In addition to this, a slight shift of peak at $2\theta \sim 26.5°$ to $2\theta \sim 26.2°$ upon exfoliation indicates an increase in inter-planar distance. This is assigned to the intercalation of $[C_{16}mim][ZnCl_3]$ between the graphene layers.[22] The absence of any diffraction peak at $2\theta \sim 10°$ suggests the exfoliation of non-oxidized graphene sheets.

As the electronic properties of graphene are sensitive to graphene quality[23,24] it is crucial to determine the quality of the exfoliated graphene sheets by Raman and X-ray photon spectroscopy (Fig. 1C and D). Raman spectra (Fig. 1C) of raw graphite and exfoliated graphene sheets show three characteristic bands at 1353, 1578 and 2731 cm^{-1} corresponding to D, G

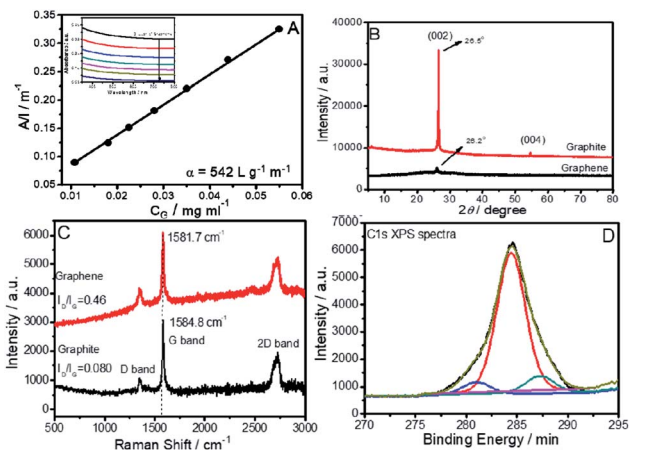

Fig. 1 (A) Absorbance per unit length (A/l) at 660 nm as a function of graphene concentration; (B) XRD pattern; (C) Raman spectra of exfoliated graphene sheets and raw graphite; (D) C 1s XPS spectra of an exfoliated graphene sheet. Inset of (A) shows the absorbance spectra of graphene at different concentrations.

and 2D bands, respectively. The ratio of D (corresponding to the presence of sp^3 defects) and G bands (corresponding plane vibration of sp^2 bonded carbon atoms), (I_D/I_G), is a measure of edge or basal defects.[24] The low value of I_D/I_G, (0.46) indicates that exfoliated graphene sheets are of good quality with low defect content in comparison to literature reports for graphene ($I_D/I_G \sim 0.27$–2.0) prepared by the liquid-phase exfoliation method.[16,20,25] The I_D/I_G value for exfoliated graphene is also lower than that observed for graphene oxide prepared by Hummer's method ($I_D/I_G = 1.1$–1.5).[26] The shifting of the position of the G band from 1584.8 cm^{-1} to 1581.7 cm^{-1} while going from graphite to graphene is assigned to the interaction of the hydrophobic part of $[C_{16}mim][ZnCl_3]$ with the graphene sheets.[24] The 2D band shape reveals that exfoliated graphene has an average thickness of about 5 layers.[27]

XPS spectra (Fig. 1D) of exfoliated graphene sheets shows a sharp peak at 284.4 eV corresponding to C–C groups,[18a] indicating that carbon atoms in graphene sheets are present in the sp^2 hybridized form. The deconvolution of the peak shows the presence of two small peaks at 280.9 eV and 287.2 eV, respectively, corresponding to C–Zn and C–O bonding, respectively.[28] These bands might come from a small amount of intercalated $[C_{16}mim][ZnCl_3]$ and methanol employed for washing of graphene sheets.

The graphene dispersion is found to be stable against agglomeration for at least 30 days, as indicated by a negligible change in the observed zeta (ζ)-potential value (+42.1 mV) (Fig. S2, ESI†) during this period. $[C_{16}mim][ZnCl_3]$ binds with exfoliated graphene *via* hydrophobic and π–π interactions. This prevents the graphene from re-aggregation and keeps the graphene suspended in aqueous solution *via* electrostatic repulsions between cationic head groups of the SAIL. Resonance peaks of various protons of $[C_{16}mim]^+$ in an aqueous dispersion of graphene exhibit a downfield shift (Fig. S3, ESI†) as compared to those of aqueous $[C_{16}mim][ZnCl_3]$ solution. This supports the adsorption of $[C_{16}mim][ZnCl_3]$ on the surface of graphene.

Further, the appearance of correlation peaks between different protons of the SAIL in an aqueous dispersion of graphene, which are absent in an aqueous SAIL, in 2D ^1H–^1H NOESY spectra (Fig. S4, ESI†) shows the presence of through-space interactions between different sets of protons of the SAIL. This is only possible *via* adsorption of $[C_{16}mim]^+$ onto the surface of graphene, which brings ionic moieties close to each other. Similar observations have also been reported earlier.[20] The TEM image (Fig. 2A) of exfoliated graphene sheets shows a wrinkled surface of exfoliated graphene. The SAED pattern (inset of Fig. 2A) shows the presence of a six-fold symmetric diffraction pattern, which corresponds to the hexagonal pattern of graphene.[24] The HR-TEM image (Fig. 2B) taken from the edge of the graphene sheet shows an interplanar distance of 0.34 nm corresponding to the (002) lattice plane of graphene. The HR-TEM image indicates that the exfoliated graphene sheets are 8–10 layers thick. AFM measurements provide insight into the dimensions of exfoliated graphene sheets (Fig. 2C–E). 4% of graphene sheets having a thickness less than 0.5 nm (mono layered) and 34% of graphene sheets with a thickness between 0.5 and 1 nm (1–3 layered graphene sheets) are observed from topological analysis of AFM images. AFM measurements

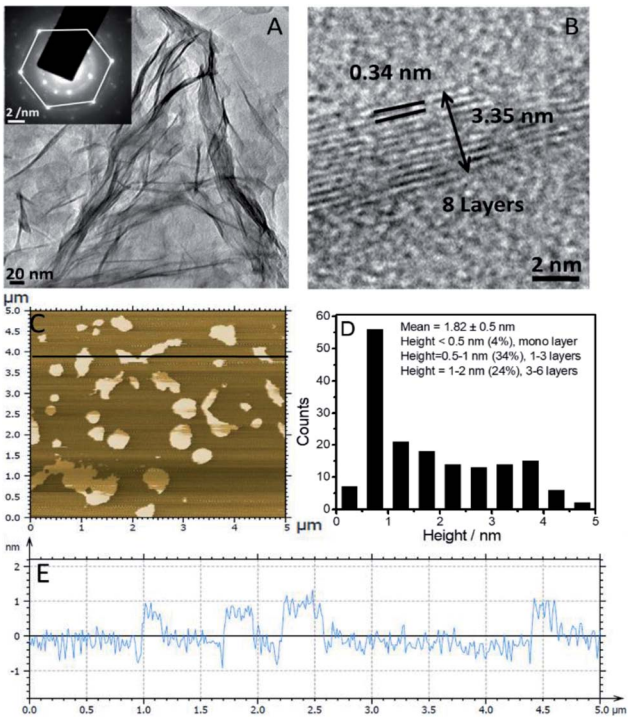

Fig. 2 (A) TEM image of an exfoliated graphene sheet; (B) HR-TEM of an edge of the graphene sheet. (C) AFM image of the exfoliated graphene sheet; (D) statistical data obtained for the height of exfoliated graphene sheets; (E) surface topography of graphene sheets. Inset of (A) shows the SAED pattern of the graphene sheet.

revealed that 56% and 52% of graphene sheets are less than 125 nm in length and 75 nm in width, respectively (Fig. S5, ESI†).

Following the exfoliation and characterization, the dispersion of graphene in aqueous $[C_{16}mim][ZnCl_3]$ is used for *in situ* preparation of ZnS QD decorated exfoliated graphene sheets (ZnS@G). Three diffraction peaks in the case of the ZnS@G NCs at the $2\theta \sim 28.4°$, $47.8°$, and $55.6°$ indexed to the 111, 220, and 311 diffraction planes of ZnS respectively, are observed (Fig. 3A).

This indicates the formation of a cubic zinc blende structure (JCPDS card no. 80-0020). The presence of a small peak at $2\theta \sim 26.1°$ in the case of ZnS@G corresponds to exfoliated graphene sheets.[24] There is no significant change in intensity and broadness of peaks corresponding to ZnS in the case of ZnS@G NCs. This indicates that the presence of graphene does not affect the size and crystallinity of ZnS QDs. Raman spectra (Fig. 3B) of the prepared ZnS@G NCs show transverse-optical (TO) and longitudinal-optical (LO) bands of ZnS below 500 cm^{-1},[29] while the bands at ~1346 cm^{-1} and ~1580 cm^{-1} in the case of ZnS@G NCs correspond to the D and G bands of exfoliated graphene sheets respectively.[24] A slight increase in the I_D/I_G value from 0.46 in the case of graphene to 0.60 in the case of ZnS@G is assigned to binding and embedding of ZnS QDs between graphene sheets (Fig. S6, ESI†). It is important to mention that ZnS QDs not only decorate the surface of graphene but also form between graphene layers. The formed ZnS QDs between graphene layers are found to be relatively smaller in size as compared to those present at the surface of graphene.

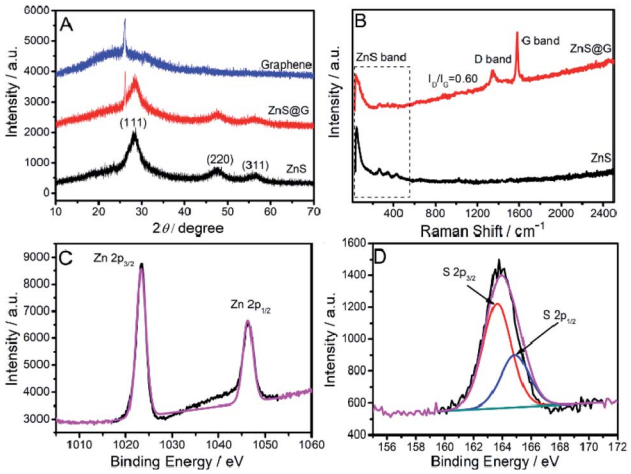

Fig. 3 (A) XRD spectra; (B) Raman spectra of the prepared ZnS@G composites and ZnS QDs; (C and D) Zn 2p and S 2p XPS spectra of the prepared ZnS@G composites respectively.

The Zn 2p XPS spectra (Fig. 3C and D) of the NCs exhibit two peaks at 1023.3 and 1046.4 eV, ascribed to Zn $2p_{3/2}$, and Zn $2p_{1/2}$ spin–orbit peaks of ZnS, respectively (Fig. 3C), while S 2p XPS spectra show bands at 163.6 and 164.9 eV, which correspond to S $2p_{3/2}$ and S $2p_{1/2}$ spin–orbit peaks, respectively.[13] UV-Vis absorbance spectra (Fig. 4A) of the prepared ZnS and ZnS@G, show a characteristic band of ZnS at ~302 nm corresponding to inter-band transition.[30]

Band-gap values for the prepared materials were calculated by extrapolation of Tauc's plot (inset of Fig. 4A) between energy (eV) and $(Ahv)^2$, where A is absorbance, h is Plank's constant and ν is frequency. The band-gap values calculated for ZnS and ZnS@G are 3.45 and 3.09 eV, respectively.

The lowering of the band-gap of ZnS with the introduction of graphene renders ZnS@G applicable for photocatalysis under visible light. This result is quite consistent with the literature reports[10–12,31,32] where a decrease in the band-gap value has been observed upon the coupling of graphene with semiconductors. This coupling suggests the charge transfer process at the ZnS/graphene interface. Further, the photoluminescence (PL) spectra (Fig. 4B) of prepared materials are recorded by excitation at $\lambda \sim 320$ nm, which shows three peaks at ~364 nm, ~403 nm and ~435 nm in the case of ZnS QDs, while the PL band is quenched in the case of ZnS@G NCs. It is well established that in semiconductor ZnS QDs, the photoemission occurs by the recombination of electrons and holes *via* different pathways.[31] Therefore, the quenching of PL bands, with the introduction of graphene, in ZnS QDs, is due to the hindrance of the recombination of electrons and holes. This results in high electron density in the conduction band of ZnS, which thus contributes to the photocatalytic enhancement.[10] This is supported by a hindered recombination of photogenerated charge carriers of ZnS in the presence of graphene as suggested by quenching of PL. Moreover, graphene provides a high surface area for the adsorption of dye molecules as indicated by a decrease in absorbance of the RhB dye in the presence of catalysts after stirring for 30 min in the dark (Fig. S8, ESI†). This brings RhB closer to ZnS QDs adsorbed at the graphene surface and enhances the photocatalytic degradation of RhB. Recyclability of the photocatalyst has been checked (Fig. 6C). No significant change in photocatalytic efficiency has been observed up to four photocatalytic cycles. Hence, an enhancement in photocatalytic efficiency is expected. The TEM image (Fig. 5A and B) of prepared ZnS QDs in the presence and the absence of graphene sheets shows that the prepared QDs are spherical, having size <10 nm (Fig. 5C). The ZnS QDs are homogeneously distributed on the graphene sheet without any aggregation. The SAED pattern (inset of Fig. 5A) of ZnS QDs show three concentric rings indexed to (111), (220) and (311) diffraction planes of ZnS QDs. The prepared size histogram (Fig. 5C) shows that the mean particle size of QDs is 8.7 nm. The HR-TEM image (Fig. 5D) of ZnS QDs shows an interplanar distance of 0.31 nm corresponding to the (111) plane of ZnS.

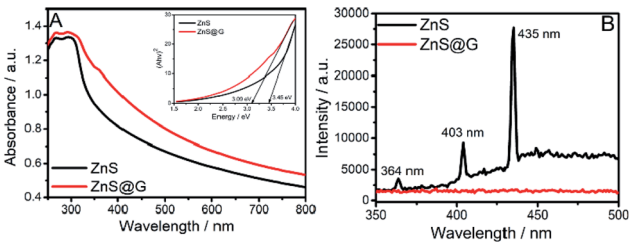

Fig. 4 (A) UV-Vis spectra; and (B) photoluminescence (PL) spectra of the prepared ZnS@G composites and ZnS QDs. Inset of (A) shows the Tauc's plot of the ZnS@G composites and ZnS QDs used to find band-gap values.

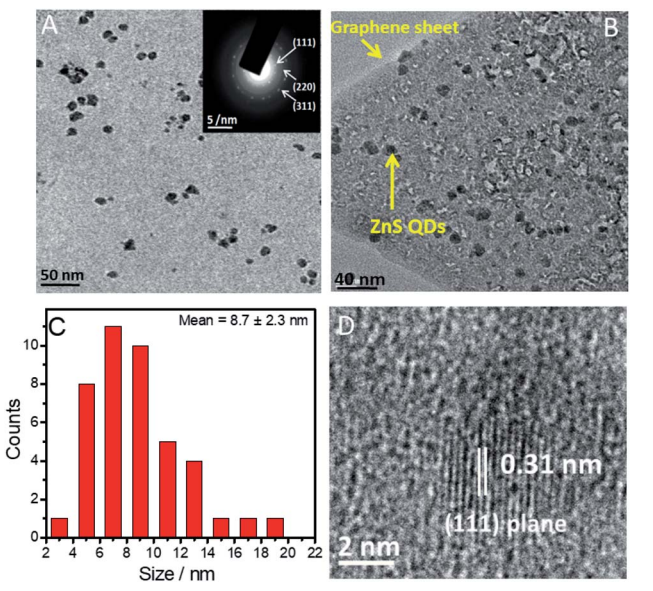

Fig. 5 (A) TEM image of the prepared ZnS QDs; (B) TEM image of the prepared ZnS@G NCs; (C) histogram showing the average size of the prepared ZnS QDs; (D) HR-TEM image of the prepared ZnS QDs. Inset of (A) shows the SAED pattern of the prepared ZnS QDs.

In the last step, the photocatalytic activities of the prepared ZnS@G NCs and their counterpart (ZnS QDs) were tested for the degradation of Rhodamine B (RhB) as a model dye under sunlight as well as an antibiotic, ciprofloxacin (CIP), under visible light. RhB shows a characteristic absorbance band at 554 nm, which decreases to a minimum in 165 min in the presence of ZnS@G (Fig. 6A). Rate constants have been calculated employing the standard first-order rate equation and are provided in Fig. 6B. ZnS@G NCs are found to be more photoactive (Fig. S7, ESI†) and show an 11 fold higher photodegradation rate in comparison to ZnS. The observed higher catalytic efficiency of ZnS@G NCs as compared to ZnS QDs could be due to a combination of different reasons.

Graphene could act as a photo-sensitizer by donating electrons to the conduction band of the semiconductor by interfacial charge transfer under sunlight irradiation. This results in high electron density in the conduction band of ZnS, which thus contributes to the photocatalytic enhancement.[10] This is supported by a hindered recombination of photogenerated charge carriers of ZnS in the presence of graphene as suggested by quenching of PL. Moreover, graphene provides a high surface area for the adsorption of dye molecules as indicated by a decrease in absorbance of the RhB dye in the presence of catalysts after stirring for 30 min in the dark (Fig. S8, ESI†). This brings RhB closer to ZnS QDs adsorbed at the graphene surface and enhances the photocatalytic degradation of RhB. Recyclability of the photocatalyst has been checked (Fig. 6C). In addition, the transient photocurrent responses of GO, ZnS and ZnS@G composites were measured under many light on–off cycles, presented in Fig. S11A (ESI†). From the results, it is clear that GO and ZnS demonstrated the lowest photocurrent response as compared to the ZnS@G hetero-junction. The introduction of ZnS onto graphene as ZnS@G composites showed excellent charge separation from the photo-generated charge carriers as compared to their counterparts. The excellent charge separation of photocatalyst was further examined by electrochemical impedance spectroscopy (EIS). Fig. S11B (ESI†) shows the Nyquist plots of the GO, ZnS and ZnS@G photo catalysts under visible-light irradiation. In the high-frequency region, the small semicircles for the ZnS@G composites evidence the smallest charge transfer resistance, which results in fast interfacial electron transfer as compared to pure counterparts. This along with the photocurrent measurements demonstrates that in the ZnS@G composites, the separation and transfer of photo-generated electrons and holes is spontaneous, which results in higher photocatalytic activity. No significant change in photocatalytic efficiency has been observed up to four photocatalytic cycles.

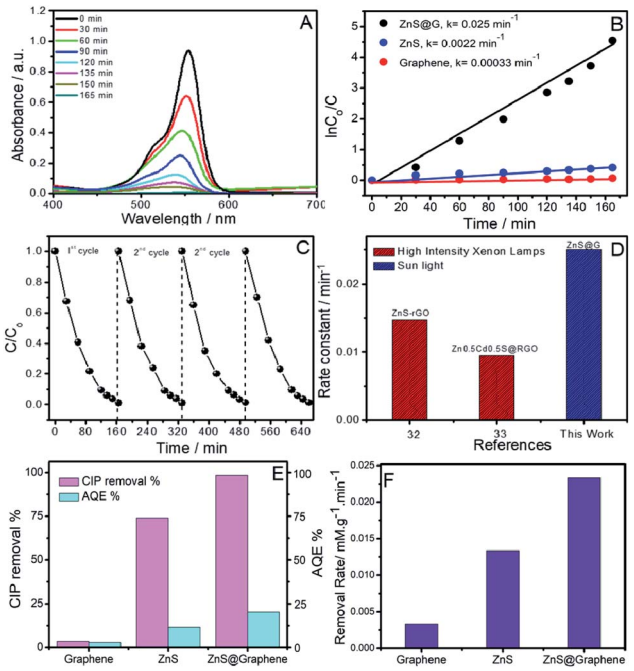

Fig. 6 (A) Time-dependent UV-Vis absorbance spectra of RhB solution in the presence of ZnS@G as a photocatalyst; (B) catalytic performances of ZnS@G, ZnS and graphene and their rate constants; (C) recyclability of the ZnS@G photocatalyst for 4 repeated catalytic cycles; (D) comparison of rate constants of ZnS@G with literature reports of graphene oxide-based composites;[32,33] (E) photocatalytic CIP removal % of graphene, ZnS and ZnS@G catalysts and their corresponding apparent quantum efficiencies (AQE) under visible light; (F) initial removal rates at 30 min for the ZnS@G catalyst and their counterparts; reaction conditions: 0.018105 mM CIP; 50 mL water; 15 mg catalyst; reaction time 30 min.

4. Conclusions

In conclusion, a sustainable and facile method for the preparation of ZnS QD decorated graphene using a zinc-containing imidazolium-based surface active ionic liquid, $[C_{16}mim][ZnCl_3]$ is reported. The reported method is different from those mentioned in the literature where either GO or rGO[10–12,32,34] was used for the preparation of ZnS based composites. The preparation of GO and rGO is a multistep process and uses many harmful chemicals. Few-layer thick graphene sheets in appreciable yield (0.6 mg mL^{-1}) and excellent colloidal stability are exfoliated using $[C_{16}mim][ZnCl_3]$ followed by *in situ* preparation of ZnS@G NCs at room temperature. The coupling of defect-free non-oxidized graphene with ZnS alters the bandgap of ZnS, thereby making it a visible light active photocatalyst. The prepared NCs show efficient photocatalytic activity for the degradation of the RhB dye and CIP antibiotic under sunlight/visible light. The present study, along with previous reports on semiconductors[35] and their composites with graphene,[2,11,12,32,33,35–41] would open up a new window for the preparation of new graphene-based NCs employing metal-based surface-active ionic liquids for different applications.

Conflicts of interest

There are no conflicts to declare.

Acknowledgements

This work is supported by DST, Govt. of India, wide project number SB/FT/CS-057/2013. Komal is thankful to UGC, Govt. of India, for the award of SRF. The infrastructure facility provided

for this work under the UPE, DST-PURSE, and CAS grant is highly acknowledged.

Notes and references

1 P. Sivakumar and P. N. Palanisamy, *Rasayan J. Chem.*, 2008, **1**, 871–883.
2 V. Diwan, A. J. Tamhankar, M. Aggarwal, S. Sen, R. K. Khandal and C. S. Lundborg, *Curr. Sci.*, 2009, **97**, 1752–1755.
3 S. Zhu and D. Wang, *Adv. Energy Mater.*, 2017, **7**, 1700841.
4 T. Frecker, D. Bailey, X. Arzeta-Ferrer, J. McBride and S. J. Rosenthala, *ECS J. Solid State Sci. Technol.*, 2016, **5**, R3019–R3031.
5 W. Q. Peng, S. C. Qu, G. W. Cong, X. Q. Zhang and Z. G. Wang, *J. Cryst. Growth*, 2005, **282**, 179–185.
6 S. Adachi, Cubic Zinc Sulphide (β-ZnS), in *Optical Constants of Crystalline and Amorphous Semiconductors*, Springer, Boston, MA, 1999.
7 H. N. Tien, V. H. Luan, L. T. Hoa, N. T. Khoa, S. H. Hahn, J. S. Chung, E. W. Shin and S. H. Hur, *Chem. Eng.*, 2013, **229**, 126–133.
8 D. Reddy, J. Choi, S. Lee, R. Ma and T. K. Kim, *RSC Adv.*, 2015, **5**, 18342–18351.
9 A. K. Sahoo, S. K. Srivastava, P. K. Raul, A. K. Gupta and R. Shrivastava, *J. Nanopart. Res.*, 2014, **16**, 2473.
10 Y. Zhang, N. Zhang, Z.-R. Tang and Y.-J. Xu, *ACS Nano*, 2012, **12**, 9777–9789.
11 M.-Q. Yang and Y.-J. Xu, *J. Phys. Chem. C*, 2013, **117**, 21724–21734.
12 A. Du, Y. H. Ng, N. J. Bell, Z. Zhu, R. Amal and S. C. Smith, *J. Phys. Chem. Lett.*, 2011, **2**, 894–899.
13 M. Mao, L. Jiang, L. Wu, M. Zhang and T. Wang, *J. Mater. Chem. A*, 2015, **3**, 13384–13389.
14 C. Li, D. Jiang, L. Zhang, J. Xia and Q. Li, *Langmuir*, 2012, **28**, 9729–9734.
15 S. W. Hummers and R. E. Offeman, *J. Am. Chem. Soc.*, 1958, **6**, 1339.
16 P. Wasserscheid and T. Welton, *Ionic Liquid in Synthesis*, Wiley, New York, 2003.
17 (*a*) K. S. Rao, P. Bharmoria, T. J. Trivedi and A. Kumar, *Self-Assembly of Surface-Active Ionic Liquids in Aqueous Medium*, Wiley, New York, 2015; (*b*) T. Singh and A. Kumar, *J. Phys. Chem. B*, 2007, **111**(27), 7843–7851.
18 (*a*) M. Lotya, Y. Hernandez, P. J. King, R. J. Smith, V. Nicolosi, L. S. Karlsson, F. M. Blighe, S. De, Z. Wang, I. T. McGovern, G. S. Duesberg and J. N. Coleman, *J. Am. Chem. Soc.*, 2009, **131**, 3611–3620; (*b*) M. Cao, N. Wang, L. Wang, Y. Zhang, Y. Chen, Z. Xie, Z. Li, E. Pambou, R. Li, C. Chen, F. Pan, H. Xu, J. Penny, J. R. P. Webster and J. R. Lu, *J. Mater. Chem. B*, 2016, **4**, 152–161; (*c*) M. Lotya, P. J. King, U. Khan, S. De and J. N. Coleman, *ACS Nano*, 2010, **4**, 3155–3162; (*d*) S. Wang, M. Yi and Z. Shena, *RSC Adv.*, 2016, **6**, 56705–56710.
19 T. Kim, H. Lee, J. Kim and K. S. Suh, *ACS Nano*, 2010, **4**, 1612–1618.
20 M. Kaur, G. Singh, K. Damarla, G. Singh, H. Wang, J. Wang, V. K. Aswal, A. Kumar and T. S. Kang, *Phys. Chem. Chem. Phys.*, 2020, **22**, 169–178.
21 D. Nuvoli, L. Valentini, V. Alzari, S. Scognamillo, S. Bittolo Bon, M. Piccinini, J. Illescas and A. Mariani, *J. Mater. Chem.*, 2011, **21**, 3428–3431.
22 R. Su, S. F. Lin, D. Q. Chen and G. H. Chen, *J. Phys. Chem. C*, 2014, **118**, 12520–12525.
23 D. S. L. Abergel and V. I. Fal'ko, *Phys. Rev. B: Condens. Matter Mater. Phys.*, 2007, **75**, 155430–155435.
24 X. Wang and P. Wu, *ACS Appl. Mater. Interfaces*, 2018, **10**, 2504–2514.
25 P. Ramalingam, S. T. Pusuluri, S. Periasamy, R. Veerabahu and J. Kulandaivel, *RSC Adv.*, 2013, **3**, 2369–2378.
26 S. Claramunt, A. Varea, D. López-Díaz, M. M. Velázquez, A. Cornet and A. Cirera, *J. Phys. Chem. C*, 1015, **119**, 10123–10129.
27 S. Parka, A. Reina, R. Saito, J. Kong, G. Dresselhaus and M. S. Dresselhaus, *Carbon*, 2009, **47**, 1303–1310.
28 C. Shen, L. Wang, A. Zhou, B. Wang, X. Wang, W. Lian, Q. Hu, G. Qin and X. Liu, *Nanomaterials*, 2018, **8**, 80.
29 M. Sookhakian, Y. M. Amin, R. Zakaria, W. J. Basirun, M. R. Mahmoudian, B. Nasiri-Tabrizi, S. Baradaran and M. Azarang, *J. Alloys Compd.*, 2015, **632**, 201–207.
30 M. Mao, L. Jiang, L. Wu, M. Zhang, T. Wang, S. M. Scholz, R. Vacassy, J. Dutta and H. Hofmann, *J. Appl. Phys.*, 1998, **83**, 7860.
31 S. P. Adhikari, G. P. Awasthi, H. J. Kim, C.-H. Park and C. S. Kim, *Langmuir*, 2016, **32**, 6163–6175.
32 S. Singh and N. Khare, *RSC Adv.*, 2015, **5**, 96562–96572.
33 A. Murugadoss and A. Chattopadhyay, *Bull. Mater. Sci.*, 2008, **31**, 533–539.
34 X.-F. Zhang, Y. Chen, Y. Feng, X. Zhang, J. Qiu, M. Jia and J. Yao, *J. Alloys Compd.*, 2017, **705**, 392–398.
35 (*a*) X. Liu and C. Chen, *Mater. Lett.*, 2020, **261**, 127127; (*b*) C. Chen, X. Liu, Q. Fang, X. Chen, T. Liu and M. Zhang, *Vacuum*, 2020, **174**, 109198.
36 S. Thangavel, K. Krishnamoorthy, S.-J. Kim and G. Venugopala, *J. Alloys Compd.*, 2016, **683**, 456–462.
37 I. Hayder, I. A. Qazi, M. A. Awan, M. A. Khan and A. Turabi, *J. Appl. Pharm.*, 2012, **1**, 487–497.
38 Y. Xu, Z. W. Liu, Y. L. Xu, Y. Y. Zhang and J. L. Wu, *J. Exp. Nanosci.*, 2014, **9**, 415–420.
39 W. Duan, A. Li, Y. Chen, K. Zhuo, J. Liu and J. Wang, *J. Nanopart. Res.*, 2018, **20**, 287.
40 H. Zhang, Y. Shang, T. Zhang, K. Zhuo and J. Wang, *Sens. Actuators, B*, 2017, **242**, 492–501.
41 S. Yang, K. Zhuo, D. Sun, X. Wang and J. Wang, *J. Colloid Interface Sci.*, 2019, **543**, 263–272.

